FREE FORM ELECTRODE-SKIN CONTACT IMPEDANCE MODEL FOR ELECTRICAL IMPEDANCE TOMOGRAPHY

Olavo Luppi Silva, olavo.luppi@usp.br
Erick Dario Leon Bueno de Camargo, edlbcamargo@yahoo.com.br
Raul Gonzalez Lima, lima.raul@gmail.com
University of So Paulo, Polytechnic School, Department of Mechanical Engineering, Av. Prof. Luciano Gualberto, 2231 CEP: 05508-900, So Paulo/SP

Abstract. *Electrical Impedance Tomography (EIT) is a technique employed to image an object internal resistivity distribution using electric current injection and voltage measurements. Among other applications, it can be used as a non-invasive medical imaging technique to obtain real time images of the lungs. Measured data is used as boundary conditions to solve Laplace equations with finite element method using a mesh of the thorax. The image thus, is itself a solution of an inverse problem, in which an iterative algorithm searches a resistivity distribution that minimizes the difference between the solution of direct problem (i.e. given resistivity distribution and applied currents, compute nodal potentials) and measured potentials. Measured voltage drops are due to both internal and boundary contact impedance. Since in clinical applications of EIT electrode-skin impedance is high, its contribution to measured voltage is significant and therefore it should be modeled. The traditional approach to this problem is to model the electrode with two hexahedrical elements whose dimensions are similar to electrode dimensions. Proceeding this way, it is difficult to refine the mesh close to them. In order to more accurately describe electric potentials close to skin, a finite element model of electrode contact impedance with tetrahedrical elements is presented. The approach describes the electrode with any number of elements which allows modeling them with different forms (circular, oblong, etc) within the desired refinement. Different possibilities of electrode modelling are discussed and one of them is implemented. An image of resistivity distribution of the lungs is obtained with and without the use of electrode model and comparisons are made.*

Keywords: *electrical impedance tomography, finite element model, contact impedance, electrode, inverse problem*

1. INTRODUCTION

Electrical Impedance Tomography (EIT) is a non-invasive technique employed to estimate the internal resistivity distribution within a subject or object. It uses an array of electrodes attached to the boundary (or skin). The electrodes are used to inject current and measure potentials in order to solve a non linear ill-posed inverse problem. EIT has both medical and industrial applications, such as monitoring lung function (Victorino et al, 2004), detect breast tumors (Bayford, 2006), obtain information on three-dimensional material distribution within process vessels (Heikkinen et al, 2006), monitoring mixing processes, etc.

Contact impedance is high in clinical applications (Rosell et al, 1988), because of an electrochemical effect. Electron flow is converted into ion flow at the electrode-skin interface which causes voltage drop at each electrode (Kolehmainen et al, 2008). Conversely, the ill-conditioned nature of EIT problem can produce large and wild oscillations in the estimated resistivity distribution if small errors on voltages are present. As a consequence, electrode effects should be modelled.

Although narrow (point) electrodes would simplify modeling process, wide electrodes are more suitable for EIT applications because they can provide more uniform current distribution inside the domain Ω. It has also lower contact impedance since this property is inversely proportional to the contact area (Hua et al, 1993). Nevertheless current density distribution in wide electrodes has some particular characteristics when compared to narrow electrodes: i) discretization effect (applied currents are null outside electrodes); ii) edge effect (higher current densities occur at the edges of electrodes, (Holder, 2005); iii) shunt effect (part of the injected current run near the boundary to the adjacent electrode which reduces current density at the interior of the body (Cheng et al, 1989). Cheng et al. (1989) presented general field equations that account for these three effects and demonstrated that it agrees with experimental data. Cheng's model is known as *Complete Electrode Model (CEM)*. Hua et al. (1993) showed how to solve CEM with the Finite Element Method for a 2D domain. In their approach they assume that each electrode-skin interface has a different resistivity and thus use 32 parameters to model their 32-electrode system.

The electrode model proposed by Hua et al. (1993) is modeled with two quadrangular elements, and thus the local conductivity[1] matrix depends on three parameters: thickness t, width a and interface resistivity ρ. The term $1/(\rho t)$ can be put in evidence and is referred to as "electrode parameter" because both t and ρ are unknown. An extension of Hua's model to 3D case with hexahedrical elements is straightforward and was made by Vauhkonen et al. (1999).

However, representing skin-electrode interface with only two elements per electrode limits both mesh discretization

[1]In finite element analysis the term "conductivity matrix" in the formulation of an electro-magnetic problem corresponds to "stiffness matrix" in structural problem.

and the description of electrode geometry. In this work we discuss some alternative possibilities to describe an electrode with an arbitrary number of tetrahedrons. Proceeding this way, it is also possible to model electrodes with different forms (circular, oblong, etc) within the desired refinement. One of the methods is tested with human data from a volunteer (Moura et al, 2009).

2. THEORETICAL BACKGROUND

It can be shown that, assuming simplifying hypotheses, the potential $\phi(x, y, z)$ inside a domain Ω is governed by the generalized Laplace equation (Eq. 1).

$$\nabla \cdot \left(\rho^{-1} \nabla \phi\right) = 0 \tag{1}$$

If no electrode model is present, solving Eq. 1 requires the assignment boundary conditions described at Eq. 2, where ρ is the resistivity distribution, ϕ is the scalar potential distribution, n is the outward unit normal of the boundary $\partial\Omega$ and J_i is the current density at i-*th* node.

$$\rho^{-1} \frac{\partial \phi}{\partial n} = \begin{cases} J_i & \text{at i-}th\text{ node} \\ 0 & \text{at the others} \end{cases} \tag{2}$$

As what is actually measured is total current I_i and not current density J_i, the boundary conditions considered are expressed at the two following Equations. Equation 3 expresses that at the area where the electrode is attached, the integral of the conductivity times the gradient of electric potential normal to the surface is the total current measured. Where there is no electrode, no current go through the surface, as shown at Eq. 4.

$$\int_{\partial\Omega_{e_i}} \rho^{-1} \frac{\partial \phi}{\partial n} dS = I_{e_i} \quad \text{at } \partial\Omega \in \text{i-}th\text{ electrode} \tag{3}$$

$$\rho^{-1} \frac{\partial \phi}{\partial n} = 0 \quad \text{at } \partial\Omega \notin \text{i-}th\text{ electrode} \tag{4}$$

What is known in the literature as Complete Electrode Model has an additional equation (Eq. 5). It says that the measured potentials at the electrodes is the potential ϕ inside the domain Ω plus a potential proportional to the contact impedance z_i times the current that goes through it $\rho^{-1}\partial\phi/\partial n$.

$$\phi + z_i \rho^{-1} \frac{\partial \phi}{\partial n} = V_i \tag{5}$$

A forward finite element problem is solved and potentials for all nodes are computed. The potentials referring to electrodes are compared to measured potentials. If the difference between these two sets of potentials are above a specified tolerance, an iterative algorithm is used, for instance Newton-Raphson (Yorkey et al. 1987), to update the resistivity of each element of the mesh. This process continues until a convergence criterion is reached.

3. THE TRADITIONAL ELECTRODE MODEL

Probably the most used electrode model by EIT community is the one proposed by Hua et al (1993), shown in Fig. 1 where the solid line, the dashed line and the diagonal stripes represent the electrode metallic part, electrode–skin contact layer and inner body underneath the barrier layer, respectivelly. The interface is modelled by two rectangular elements I and II, where a is rectangle width and t is rectangle thickness as shown at the right of Fig. 1. The potentials within the elements are considered piece–wise linear. Imposing the same potential to all nodes of metallic part (see Appendix), Hua et al (1993) proposed the conductivity matrix shown at Eq. 6.

$$\frac{1}{3at\rho} \begin{bmatrix} a^2+t^2 & \frac{a^2}{2}-t^2 & 0 & -\frac{3a^2}{2} \\ & 2\left(a^2+t^2\right) & \frac{a^2}{2}-t^2 & -3a^2 \\ & & a^2+t^2 & -\frac{3a^2}{2} \\ & sym & & 6a^2 \end{bmatrix} \begin{bmatrix} \phi_1 \\ \phi_2 \\ \phi_3 \\ \phi_4 \end{bmatrix} = \begin{bmatrix} 0 \\ 0 \\ 0 \\ I_i \end{bmatrix} \tag{6}$$

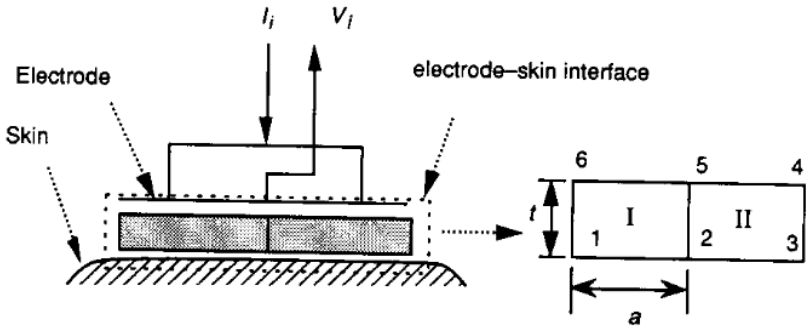

Figure 1. Traditional electrode model proposed by Hua et al. 1993

However it is convenient to estimate a single electrode parameter defined by ρt. Hua et al. (1993) argued that, when the elements of an electrode are large, a simplification can be made, neglecting t^2 in Eq. 6. The resulting Equations 7 constitute what the authors call the Traditional Electrode Model.

$$\frac{1}{3t\rho}\begin{bmatrix} a & \frac{a}{2} & 0 & -\frac{3a}{2} \\ & 2a & \frac{a}{2} & -3a \\ & & a & -\frac{3a}{2} \\ & sym & & 6a \end{bmatrix}\begin{bmatrix}\phi_1\\ \phi_2\\ \phi_3\\ \phi_4\end{bmatrix} = \begin{bmatrix}0\\0\\0\\L\end{bmatrix} \tag{7}$$

4. METHODOLOGY

4.1 Mesh generation

The mesh of a human thorax section with 0.06 m thickness is shown in Figure 2. It has 2025 nodes and 8814 tetrahedrical elements and was generated by GMSH (Geuzaine and Remacle, 2009). There are 32 circles aligned at the same plane of mesh boundary that represents the area where the electrodes are attached, each one having an average of 14 tetrahedral faces. The size of the tetrahedrons behind electrodes is about $1/6$ of the elements in the middle of the domain. As the resistivity of elements belonging to electrodes change slowly in time, they can be calculated with certain periodicity. In the present work electrode resistivity and thickness was kept constant.

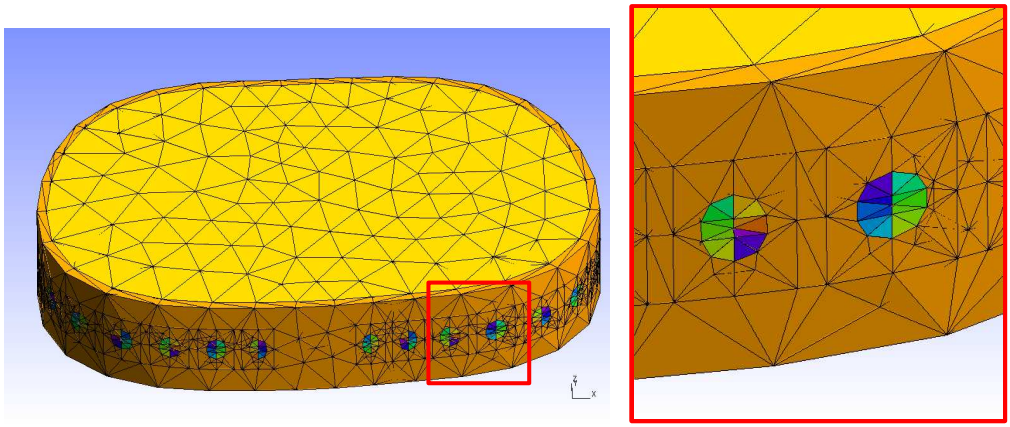

(a) Example of finite element mesh representing a section of human thorax.

(b) Detail of the discretization of the electrode region.

Figure 2. Mesh

4.2 Possibilities of a simplified electrode model

The equations 1 and 3–5 are general field equations and are considered the most accurate model for EIT (Somersalo et al. 1992). One of the most suitable ways to numerically solve these field equations for arbitrary geometry is using the Finite Element Method. A complete demonstration of how to go from field equations to system of equations in order to solve FEM direct problem is beyond the scope of this work and can be found at Hua et al. (1992) and Vauhkonen et al. (1999).

In this work, the authors would like to propose four different possibilities to model the skin–electrode interface. First–order basis functions are used to calculate its associated local conductivity matrix. The main difference between the tradditional electrode model and the proposed models is that our models do not assume that $t << a$ on Eq. 6. Proceeding this way, t^2 is not neglected and more refined meshes can be used.

Figure 2(b) shows an electrode modeled with 14 triangular elements. When applying boundary conditions (Eq. 3), and no electrode model is present, it is necessary to choose one single node where the current will be injected and another node where all current will be drained, while all other nodes at $\partial\Omega$ should have null current. This approach causes an underestimation of the resistivity distribution.

Model 1

Now suppose a local conductivity matrix of an electrode formed by four triangles is to be constructed. One of the possibilities is to add an additional "virtual" node outside the mesh and construct four additional tetrahedrons, as shown in Figure 3(a). The height of this virtual node is small (in fact, a fraction of a millimeter) because the potential drop at the interface between skin and electrode is to be modeled. This model is not adequate because the metal part of the electrode is not represented and the resistance from the injecting node to the skin varies within the electrode model. If the current tries to go from injection node to the extremity of the electrode, it will face a resistance larger than if it goes in the direction perpendicular to the skin.

Model 2

Another possibility is to add a "virtual" node per triangle, such that a new tetrahedron will be formed for each triangle of the electrode, Figure 3(b). Four "virtual" nodes will be generated. There are four tetrahedrons for the flow of current and the non-uniform resistance problem noted in *Model 1* is reduced. How much current should be set to each 'virtual" node? To divide the total current per number of nodes is not adequate. Holder (2005) shows that current density distribution is not uniform near the electrode. Since the difference of potentials between all *virtual nodes* and skin are not equal, it is no longer correct to impose that the currents injected to the "virtual nodes" are the same.

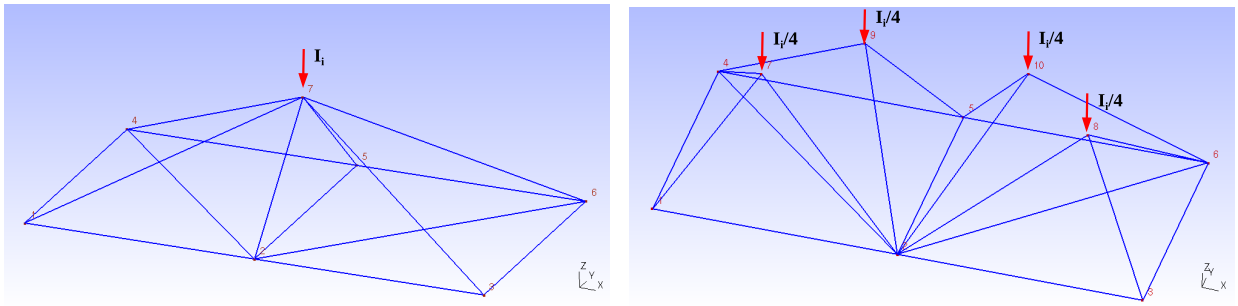

(a) Model 1: Electrode with 4 tetrahedrons and a single injection node (b) Model 2: Electrode with 4 tetrahedrons and multiple injection nodes

Figure 3. Poor electrode models

Model 3

One form to improve *Model 2* is to connect all virtual nodes with a infinitely conducting wire as shown in Figure 4(a). It imposes a constraint that all "virtual nodes" have the same electric potential. And it is no longer necessary to make conjectures about how much current should be set to each virtual node.

Model 4

It may be sad that *Model 3* does not represent correctly the "volume" of the electrode. In fact, what we are trying to model is the effect of the electrode–skin interface, which has virtually no volume. In the same way as the metal part of the electrode was modeled in *Model 3*, it is possible to connect the virtual nodes by a conducting wire. Again, all "virtual nodes" will be set to have the same potential. The electrode is formed by pentahedrons as shown in Figure 4(b). As each pentahedron can be formed by three tetrahedrons, no additional significant effort is required to implement this model.

4.3 Setting node potentials

The proposed models consider that all "virtual nodes" have the same potential. Considering Fig. 4(b), which has 12 nodes, the corresponding hyper–element conductivity matrix will have a size of 12x12. When the nodes of the upper external face are connected by a perfectly conducting wire, the hyper–element conductivity matrix is reduced to 7x7. The algebraic details of this transformation is described in the Appendix.

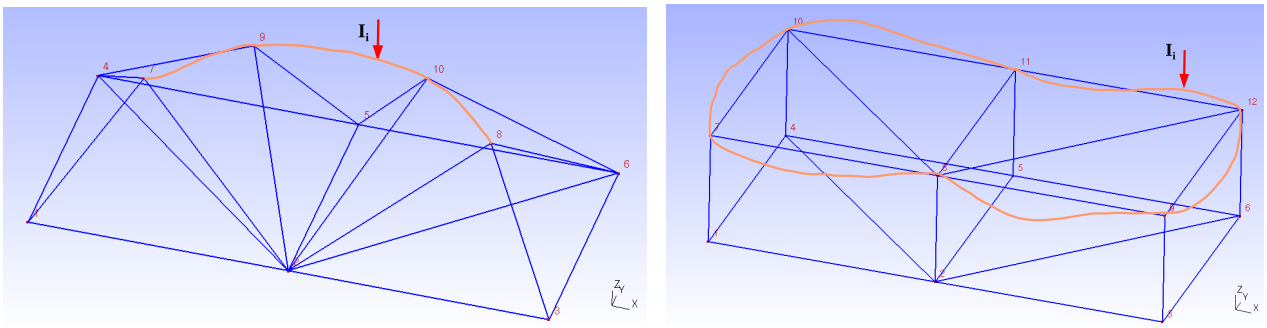

(a) Model 3: Electrode with 4 tetrahedrons

(b) Model 4: Electrode with 4 pentahedrons each one formed by 3 tetrahedrons

Figure 4. Good electrode models (with short-circuited multiple injection nodes)

5. RESULTS

The results where processed in a computer with two physical Intel Xeon Dual Core 3.0 Ghz processors with 4.0 Gb of RAM, running Fedora 10 Linux distribution. The algorith was written in C programing language using Intel Math Kernel Library (MKL) and compiled with GCC version 4.3.2. The execution time to obtain each image was about 30 minutes. The following images represent tissue resistivity in gray scale, obtained using a Newton-Raphson based algorithm. Each electrode is formed by 42 tetrahedrons, or 14 pentahedrons. Resistivity is assumed constant inside each element. Linear interpolation of resistivity at the center of the elements was used to generate the following images.

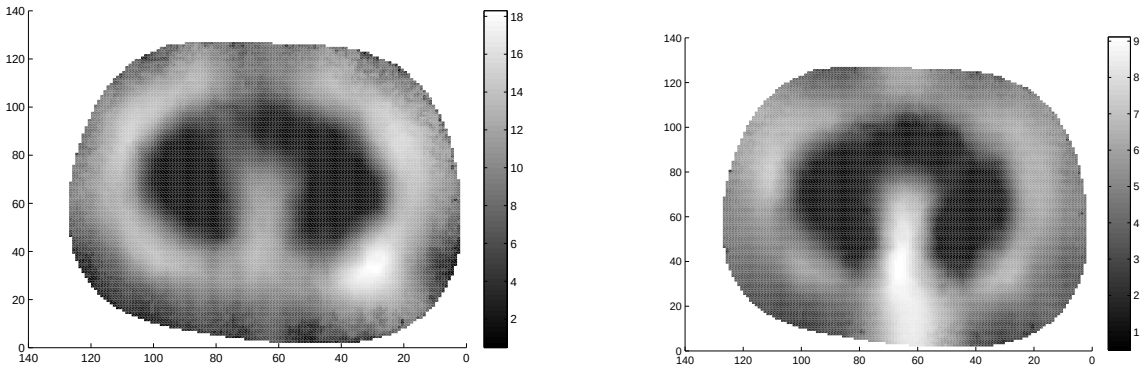

(a) Using electrode model (*model 4*)

(b) Not using electrode model

Figure 5. Estimated resistivity distribution of a human thorax

Figure 5(a) shows the estimated resistivity distribution of a human thorax when the electrode *Model 4* is used. The spinal column is at the bottom of the image. Lungs are represented by the dark areas. The ribcage, formed by the surrounding lighter areas, is visible but appear with overestimated width.

Figure 5(b) shows the estimated resistivity distribution using the same finite elements mesh when no electrode model is used. The spinal column and the ribcage have resistivities lower than in Figure 5(a). The lungs are represented by dark regions. Both images are underestimating the values of tissue resistivity, probably due to non-ideal hardware behaviour and inadequate mesh refinement.

6. DISCUSSION

The ribcage width seems overestimated taking into account anatomical knowledge. The overestimation of the ribcage width may suggest that an even more refined mesh should be used. However, increasing the mesh refinement causes an increase in computational cost. The Random Access Memory (RAM) is totally occupied and the swap area in the hard disk begins to be used, significantly increasing the computational time. This fact prevented the use of a more refined mesh.

The electrode models presented by Hua et al (1993) and Vauhkonen et al. (1999) depend on mesh refinement. They are acceptable only if $t << a$ (see Fig. 1 and Eq. 6). As a consequence of the discontinuity between skin and metal resistivities, the low degree of the interpolation polynomials within the tetrahedrons and the high electric potential gradients near the skin/electrode interface, are normally not well represented by course electrode models. One way to

overcome this problem is to refine both domain and electrode meshes. However if electrode mesh if finelly refined, the assumption of $t << a$ is no longer valid and the simplification of the traditional electrode model (Eq. 7) becomes innacurate. Therefore, Model 3 and 4 are potentially more accurate because they can be more refined.

Furthermore since some of the electrodes for EIT nowadays are not made by a metal plate, but a web of fine conducting wires, Model 4 and 3 are better than the ones that assume $t << a$ because a more refined mesh can be used.

The results of Figure 5(b) and 5(a)

The difference between Figure 5(b) and 5(a) is that the electrode model of the second image better represents the low resistivity of the metal. From the practical point of view, the use of *Model 4* generates a more conductive electrode model. As a consequence, the domain presents higher resistivities and in closer agreement with the published data (Gabriel et al, 1996). The results suggest that more refined electrode models propperly representing the metal component could increase the accuracy of the estimated resistivities of the tissues.

7. APPENDIX

The relation between potentials and nodal currents, in Finite Elements Method, is given by $\mathbf{KV} = \mathbf{I}$, where $\mathbf{K}$ is the conductivity matrix, $\mathbf{V}$ is the nodal potentials vector and $\mathbf{I}$ os the current vector in each node. To explain the algebraic procedure to impose equal electric potential to several nodes, consider a simple conductivity matrix with size 3x3, for the sake of simplicity, shown at Eqs. 8.

$$\begin{array}{rcl} k_{(1,1)}v_1 + k_{(1,2)}v_2 + k_{(1,3)}v_3 &=& I_1 \\ k_{(2,1)}v_1 + k_{(2,2)}v_2 + k_{(2,3)}v_3 &=& I_2 \\ k_{(3,1)}v_1 + k_{(3,2)}v_2 + k_{(3,3)}v_3 &=& I_3 \end{array} \tag{8}$$

If we impose $v_2 = v_3 \equiv v$, with v unknown, Eq. 8 can be written as:

$$\begin{array}{rcl} k_{(1,1)}v_1 + (k_{(1,2)} + k_{(1,3)})v &=& I_1 \\ k_{(2,1)}v_1 + (k_{(2,2)} + k_{(2,3)})v &=& I_2 \\ k_{(3,1)}v_1 + (k_{(3,2)} + k_{(3,3)})v &=& I_3 \end{array} \tag{9}$$

Summing the second and third rows,

$$\begin{array}{rcrcl} k_{(1,1)}v_1 & + & (k_{(1,2)} + k_{(1,3)})v & = & I_1 \\ (k_{(2,1)} + k_{(3,1)})v_1 & + & [(k_{(2,2)} + k_{(2,3)} + (k_{(3,2)} + k_{(3,3)})]v & = & I_2 + I_3 \end{array} \tag{10}$$

is easy to see that Eqs. 10 can be written in matrix form (Eq. 11). Observe that now the conductivity matrix is a 2x2 matrix. In this way, the procedure to obtain the local conductivity matrices of an electrode was explained.

$$\left[\begin{array}{cc} k_{(1,1)} & k_{(1,2)} + k_{(1,3)} \\ k_{(2,1)} + k_{(3,1)} & (k_{(2,2)} + k_{(2,3)} + (k_{(3,2)} + k_{(3,3)}) \end{array} \right] \cdot \left[\begin{array}{c} v_1 \\ v \end{array} \right] = \left[\begin{array}{c} I_1 \\ I_2 + I_3 \end{array} \right] \tag{11}$$

8. ACKNOWLEDGEMENTS

The authors gratefully acknowledge CAPES and CNPq for financial support.

9. REFERENCES

Bayford, R. H., 2006, "Bioimpedance tomography (Electrical impedance tomography)", Annu. Rev. Biomed. Eng., Vol. 8, pp.63–91

Cheng, K.S., Isaacson, D., Newell, J.C., Gisser, D.G., 1989, "Electrode Models for Electric Current Computed Tomography", IEEE Trans. Biomed. Eng., Vol.36, No.9, pp. 918-924.

Gabriel, C., Gabriel, S., Corthout, E., 1996, "The dielectric properties of biological tissues: I. Literature survey", Phys. Med. Biol., Vol. 41, pp. 2231–2249.

Geuzaine, C., Remacle, J.-F., 2009 "Gmsh: a three-dimensional finite element mesh generator with built-in pre- and post-processing facilities", International Journal for Numerical Methods in Engineering, Published Online: May 7 2009, DOI: 10.1002/nme.2579.

Heikkinen, L.M., Kourunen, J., Savolainen, T., Vauhkonen, P.J., J.P. Kaipio, Vauhkonen, M., 2006, "Real time three-dimensional electrical impedance tomography applied in multiphase flow imaging", Meas. Sci. Technol. Vol. 17, pp. 2083–2087

Holder, D. (Editor), 2005, "Electrical Impedance Tomography: Methods, History and Applications", Series in Medical Physics and Biomedical Engineering, Institute of Physics Publishing.

Hua, P., Woo, E.J., Webster, J.G., Tompkins, W.J., 1993, "Finite Element Modeling of Electrode-Skin Contact Impedance in Electrical Impedance Tomography", IEEE Trans. Biomed. Eng., Vol.40, No.4, pp. 335-343.

Kolehmainen, V., Lassas, M., Ola, P.,"Electrical impedance tomography problem with inaccurately known boundary and contact impedances", IEEE Trans. Med. Imaging, Vol. 27, No. 10, pp. 1404–1414.

Moura, F. S., Aya, J. C. C., Fleury, A. T., Lima, R. G., 2009, "Dynamic Imaging in Electrical Impedance Tomography of the Human Chest with Online Transition Matrix Identification", IEEE Trans. Biomed. Eng., submitted.

Rosell, J., Colominas, J., Riu, P., Pallas-Areny, R., Webster, J.G., 1988, "Skin Impedance from 1Hz to 1MHz", Trans. Biom. Eng. Vol. 35, No. 8, pp. 649-651.

Somersalo, E., Cheney, M., Isaacson, D., 1992, "Existence and Uniqueness for Electrode Models for Electric Current Computed Tomography", SIAMM J. Appl. Math, Vol.52, No.4, pp. 1023-1040.

Vauhkonen, P.J., Vauhkonen, M., Savolainen, T., Kaipio, J.P., 1999, "Three-Dimensional Electrical Impedance Tomography Based on the Complete Electrode Model", IEEE Trans. Biomed. Eng., Vol.46, No.9, pp. 1150-1160.

Victorino JA, Borges JB, Okamoto VN, Matos GF, Tucci MR, Caramez MP, Tanaka H, Sipmann FS, Santos DC, Barbas CS, Carvalho CR, Amato MB, 2004, "Imbalances in regional lung ventilation: a validation study on electrical impedance tomography", Am. J. Respir. Crit. Care Med., Vol. 169, pp. 791–800.

Yorkey, T.H., Webster, J.G., Tompkins, W.J., 1987, "Comparing reconstruction algoritms for electrical impedance imaging", Trans. Biom. Eng., Vol. BME-31, No. 11, pp. 843–852.

10. Responsibility notice

The author(s) is (are) the only responsible for the printed material included in this paper